Carbohydrate Polymer Technologies and Applications 5 (2023) 100264

Contents lists available at ScienceDirect

Carbohydrate Polymer Technologies and Applications

journal homepage: www.sciencedirect.com/journal/carbohydrate-polymer-technologies-and-applications

Performance comparison of coatings based on cellulose nanocrystals and microfibrillated cellulose for food packaging

Ghislain Fotie [a,*], Stefano Gazzotti [b,c], Marco Aldo Ortenzi [b,c], Sara Limbo [a], Luciano Piergiovanni [a]

[a] DeFENS, Department of Food, Environmental and Nutritional Sciences, Università degli Studi di Milano, Via Celoria 2, Milano 20133, Italy
[b] Dipartimento di Chimica, Università degli Studi di Milano, Via Golgi 19, 20133 Milano, Italy
[c] CRC Materiali Polimerici "LaMPo", Dipartimento di Chimica, Università degli Studi di Milano, Via Golgi 19, 20133 Milano, Italy

ARTICLE INFO

Keywords:
Cellulose nanocrystals
Microfibrillated cellulose
Coatings
Gas barrier properties
Food packaging applications
Food shelf-life extension

ABSTRACT

This article aimed at comparing gas barrier performance of plastic films coated with both cellulose nanocrystals (CNCs) and microfibrillated cellulose (MFC) obtained from cotton linters. CNCs were chemically isolated by ammonium persulfate (APS) hydrolysis, while the MFC was obtained mechanically either by APS-assisted pretreatment (MFC_{aps}) or without pretreatment (MFC). Initially, mechanical tests of the three samples were performed and their properties were characterized by dynamic light scattering, TEM, FTIR, TGA and WAXS. Subsequently, coated PET films were characterized by water contact angle, transparency and opacity evaluation following by water vapor and oxygen transmission rates assessment performed at 25 °C/ 90% RH and 25 °C/ [0%–80% RH] respectively. Finally, oxygen diffusion and solubility coefficients were calculated by using half-time method. The findings showed that, coated films based on MFC_{aps} display a much better oxygen barrier under higher RH and a higher level of residue when submitted to 700 °C degradation compared to CNCs.

1. Introduction

Today and in future, the world is called upon to face major challenges such as global warming and environmental pollution. Hence, all industrial sectors including packaging must make a serious and concrete contribution to the mitigation of these threats by adopting innovative technologies that allow the implementation of more advanced and engineered materials. Plant-based nanocellulose (NC) exhibits excellent properties that have fostered researchers and manufacturers to seek to make their application possible in many fields including food packaging. NC is generally intended as a structure having at least one dimension less or equal to 100 nm. Owing to biodegradability, non-toxicity, extraordinary mechanical and barrier properties to grease/water vapor/gases/volatile compounds, NC positions itself as a valid candidate for the replacement of oil-based barrier resins such as copolymer of Ethylene Vinyl Alcohol (EVOH), aromatic polyamide (MXD6) and Polyvinylidene Chloride (PVDC) (Dufresne, 2013). Actually, NC is generally obtained by chemical or mechanical disintegration of cellulosic raw materials after having subjected them to possible pre-treatments. NC is generally comprised of two categories such as cellulose nanocrystals (CNCs) often called nanocrystalline cellulose (NCC) and cellulose nanofibrils (CNFs) often referred to as microfibrillated cellulose (MFC) or cellulose microfibrils (MFCs). CNCs and MFC abbreviations have been generally adopted in this article. Both CNCs and MFC are smaller, more crystalline, stiffer and stronger than their parent bulk (cellulose). CNCs are generally reported to be a more crystalline and denser structure having a length of 100–250 nm and width of 3–50 nm while the MFC has a length >1 μm and width 3–100 nm displaying a much higher aspect ratio and flexibility (Xu et al., 2013). The main route to prepare CNCs is through acid hydrolysis by means of sulfuric acid (H_2SO_4) (Jiang & Hsieh, 2013). However, according to some reports, carboxylated CNCs can be produced using ammonium persulfate (APS) and 2,2,6,6-tetramethylpiperidine-1-oxyl (TEMPO) (Leung et al., 2011; Montanari et al., 2005). On the other hand, MFC is obtained mechanically either by high-pressure homogenization, cryocrushing, micro-grinding or microfluidization, each presenting advantages and shortcomings. Prior to being subjected to the top-down process, the cellulosic materials can undergo chemical, enzymatic or mechanical pretreatments in order to save energy and time during the production (Nechyporchuk et al., 2016; Ribeiro et al., 2019; Zhang et al., 2013). Lately, it has been reported an innovative method of

* Corresponding author.
E-mail address: Ghislain.Fotie@gmail.com (G. Fotie).

https://doi.org/10.1016/j.carpta.2022.100264

Available online 30 November 2022

pretreatment with APS to produce the MFC, consisting in partially fragmenting while oxidizing recalcitrant cellulosic raw materials, which is opposed to TEMPO commonly used to oxidize already produced CNFs (Filipova et al., 2018; Nair et al., 2014). As a consequence of the oxidation of the reactive hydroxyl groups, carboxylated NC suspensions display a more colloidal stability when dispersed in water and they were also found to adhere strongly to substrates such as plastics and papers (Fotie et al., 2020; Fujisawa et al., 2011; Nair et al., 2014; Aulin et al., 2010). In terms of comparison, as their thickness increases, castings based on CNFs/MFC have been reported to exhibit better flexibility and tensile strength compared to CNCs ones. However, due to lack of works on the subject, it is still under discussion which of CNCs or CNFs castings/coatings exhibit better gas barrier properties (Aulin et al., 2010). Wang and co-workers showed that, using the same cellulosic source and equal casting thickness, castings-based CNFs showed a lower O_2 permeance at 23 °C/80% RH and a higher opacity with respect to CNCs ones (Wang et al., 2020). Amongst many other NC applications such as casting-evaporation, electrospinning, extrusion, the coating technique seems to be the best technological approach in terms of functionality and sustainable applicability in large-scale packaging manufacturing. Since the crystalline lattice is well-organized and uniform within the coating, NC layers can be better embedded between substrates like papers and plastics for the implementation of high oxygen-barrier and active packaging useful for food shelf-life extension (Fotie et al., 2020; Lefatshe et al., 2017; Wang et al., 2020; Zheng et al., 2019). That being said, it is worth mentioning that one of the main obstacles preventing rapid incorporation of the NC into bio-based packaging applications is its high sensitivity to humidity which then undermines its initial mechanical properties and the barrier to gases (Fotie et al., 2017). In this investigation, a wide range of RH values was considered to understand the thermodynamic mechanisms that occur during the oxygen diffusion in the presence and absence of humidity in order to discover which between CNCs and MFC exhibits the better gas barrier properties under given conditions. Previous studies conducted on CNCs-coated PET films to investigate the influence of the RH on the gas permeabilities revealed that, O_2 and CO_2 barrier is completely lost at around 80% RH and 40% RH respectively (Fotie et al., 2017; Fotie et al., 2018). In the present work, chemical-physical properties of the CNCs and MFC have been compared in terms of size, crystallinity index, tensile strength as well as water vapor and oxygen permeabilities of coated PET films. In particular, the study of oxidized surface groups can be essential to understand their effects on thermal stability and mechanical properties. In line with current and future challenges, this article provides manufacturers with useful information that can help them to adopt innovative approaches for a rapid implementation of eco-friendly packaging materials that meet the requirements and principles of the circular economy and green chemistry (Fotie et al., 2018; Kargarzadeh et al., 2017).

2. Materials and methods

2.1. Materials

PET films (12±0.1 μm) were provided by SAPICI spa, Cernusco sul Naviglio, Italy. Cotton linters used to produce CNCs, MFC and MFCaps were kindly supplied by Innovhub (Milano, Italy). All the chemicals used were purchased from Sigma-Aldrich (Milano, Italy).

2.2. Methods

2.2.1. Optical microscopy of neat and pretreated cotton linters

Neat and APS-pretreated cotton linters were homogeneously dispersed in water at 0.8% (m/m) and observed using an optical microscope (Micro Nikon Eclipse ME600 Laboratory Imaging; Nikon Instruments, Sesto Fiorentino, Italy) at 10 × magnification. Images were captured by NIS-Element software (Nikon Instruments, Sesto Fiorentino, Italy).

2.2.2. CNCs and MFC production

CNCs were produced by APS hydrolysis according to Leung and co-workers (Leung et al., 2011; Oun & Rhim, 2018). Briefly, for CNCs production, 10 g of grinded cotton linters were suspended in distilled water, containing 1 M APS (m/V) at 75 °C and the reaction occurred under stirring conditions for 16 h. For MFC_{aps} preparation, shredded cotton linters (Ø 0.5 mm) dispersed in water at 1.5% (m/m) were sequentially pre-treated with 1 M APS (m/V) for 2 h at 35 °C, 2 h at 55 °C and 1 h at 70 °C. It can be noted that operating conditions were not severe enough to provoke a high production of nanoparticles or an important release of reactive oxidizing agents that contribute to carboxyl groups' formation on the MFC surface (Filipova et al., 2018). Subsequently, pretreated cotton linters (pH = 0.8) were washed with distilled water until pH 6–7 to discard the APS residue and nanoparticles produced. Finally, the latter was subjected to 10 min-Ultra Turrax homogenization for APS-treated suspensions to further disaggregate the microfibrils and forced them to move through a high-pressure homogenizer (GEA Lab Homogenizer, PandaPLUS 2000, Parma, Italy) for 12 passes at pressure 800–1750 bar to pop-out the MFC_{aps}. Untreated microfibrillated cellulose (MFC) was also produced without APS pretreatment but after 55 min-Ultra Turrax homogenization. Subsequently, the yield of production was calculated by using the following Eq. (1):

$$Yield(\%) = (w1 / w2)x100 \quad (1)$$

Where w1 (g) is the weight of the dried cellulose nanocrystals or microfribrillated cellulose and w2 (g) is the weight of the cotton linters used for the production.

2.2.3. Hydrodynamic diameter and Z potential evaluation

Apparent hydrodynamic diameter of water-dispersed CNCs 0.5 wt% at pH 6 was measured by using the PALS technology (mod. Litesizer 500, Anton Paar, Graz, Austria). Measures read at 90° detection angle by dynamic light scattering (DLS) (90° and 25.0 ± 0.1 °C), *via* a 35 mW diode laser (λ = 658 nm) were replicated 5 times. The actual dimensions of CNCs, MFC and MFC_{aps} were evaluated by means of Transmission Electron Microscopy (TEM). The three samples dispersed in water at 0.5 wt% were deposited on carbon-coated electron microscope grids, negatively stained with uranyl acetate and, after drying, they were analyzed by a Hitachi Jeol-10,084 TEM (Hitachi, Brugherio, Italy) operated at a voltage of 80 kV.

2.2.4. Wide angle X-ray scattering (WAXS)

Wide Angle X-ray Scattering (WAXS) experiments were performed using a Rigaku DMAX-II diffractometer (Japan). Diffraction patterns were obtained in the range $10°<2\theta<40°$with Cu Kαradiation (λ = 1.5405 Å) under the following conditions: 40 kV, 40 mA, step width 0.02°, time per step2 s, divergence slit 0.25°, Soller slit 0.04 rad and antiscatter slit 0.5°. X-ray patterns are normalized on the main peak.

2.2.5. Thermogravimetric analyses (TGA)

TGA tests were conducted (TGA 4000 Perkin Elmer, Milano, Italy) in nitrogen atmosphere on samples weighing from 5 mg to 10 mg each, with a program that provides a single heating cycle from 30 °C to 700 °C at 20 °C/min.

2.2.6. Characterization of CNCs and MFCaps surface charges

Conductometric titrations were conducted to determine the carboxylate contents of CNCs and MFC_{aps}. The apparatus is constituted of a pHmeter and conductivity meter (Multi3620 IDS) and a titrator (Si Analytics Model Titronic 300, YSI, 1725 Brannum Lane, Yellow Springs, OH, USA). 15 mg of CNCs were suspended in 200 mL of distilled water and sonicated for 5 min. The pH of the suspension was then adjusted to 3 with HCl 0.1 M before the titration with NaOH 0.01 M (0.l mL aliquots in 60 s intervals) and before determining the electric conductivity (μS/cm). For MFC_{aps}, 100 mL of 0.1% (m/m) dilute suspensions were adjusted to

pH 2.5 with 0.1 M HCl and stirred vigorously for 30 min. After, the titration was run with 0.01 M NaOH under gentle stirring and a weak equivalence point was obtained, followed by the strong one. The oxidation degree (OD, mol hydroxyl groups/mol glucose) of CNCs and MFC_{aps} was calculated using the following Eq. (2)

$$OD = [162x\ Mx(v2 - v1)]/[m - 36xMx(v2 - v1)] \quad (2)$$

where M is the NaOH concentration used for the titration, v1 and v2 expressed in L are the amount of NaOH obtained from the first and second intersection points in the titration curve respectively; m is the weight of dried samples (g); 162 and 36 represent the molecular weight of a unit of anhydro-glucose (AGU) and the difference of molecular weight between AGU and sodium salt of a gluconic acid moiety, respectively.

2.2.7. FTIR spectroscopy

The FTIR spectroscopy was performed by a Perkin Elmer instrument (Spectrum 782) equipped with ATR accessory at room temperature. The analysis was performed on all the three samples MFC, MFC_{aps} and CNCs initially brought at the same pH 6 and dried at room temperature, and the data were collected over 64 scans with resolutions of 4 cm^{-1}.

2.2.8. Tensile strength evaluation

Samples for mechanical testing were prepared as films through solvent casting deposition of water-based solution (5 wt% for CNCs, 2 wt% for MFC and MFCaps) on transparent plastic plates. Films were cut into stripes and their thickness and length were evaluated before the analysis. Film thickness was recorded with a Mitutoyo Absolute Digimatic thickness gauge. Analyses were then recorded on a MCR302 Modular Compact Rheometer (Anton Paar) at room temperature (23 °C and 50% RH) using Universal Extentional Fixture UXF12 \module. Analyses were run recording 300 points with a 0.01 min delay and increasing shear stress from 0 to 45 MPa.

2.2.9. Nanocellulose coating and thickness assessment

PET films were previously treated by corona treatment to increase their surface energy and promote their adhesion with polar substances such as CNCs and MFCaps (Johansson, 2017). Unlike the MFCaps, it was not possible to coat uniformly the MFC (obtained without APS-pretreatment) onto PET films due to its bigger dimensions. The PET films were then coated through a bar coater (K control Coater model 202, Royston, SG8 0QZ UK) to deposit one-layer of CNCs (PET-CNCs) and three layers of MFC_{aps} (PET-MFC_{aps}) both dispersed in water at 6 wt % and 2 wt% respectively. All coated PET were then stored under dry conditions (23 °C) for 48 h, and the thickness of MFCaps layer was evaluated by a 0.001 mm-resolution micrometer (QuantuMike Series 293-Coolant Proof Micrometer, USA, Illinois 60,502) and the following Eq. (3) was used:

$$L = L2 - L1 \quad (3)$$

where L (μm), L2 (μm) and L1 (μm) express the thickness of MFCaps layer, MFC-coated PET and uncoated PET respectively, collected on 4 pieces of samples. Due to the very low thickness, CNCs layer was assessed by a gravimetric method. Four samples (10 × 10 cm^2) were weighed (m1, g), then the coating was removed by washing in hot water (~70 °C), and the resulting uncoated film was dried and weighed (m2, g). The coating thickness (L, cm) was estimated by Eq. (4), where ρ is the CNCs density assumed as 1.59 g ml^{-1}:

$$L = (m1 - m2)/(\rho \times 100) \quad (4)$$

2.2.10. Water contact angles assessment

Static contact angles of the PET film coated with CNCs and MFC_{aps} were assessed. By sessile drop method, a droplet of 4.0 ± 0.5 μL of water was gently dropped onto the coated material and measurements were run at room temperature (40% RH) on five different positions for each sample. The instrument used for the measurement of the contact angle was an OCA 15 Plus angle goniometer (Data Physics Instruments GmbH, Filderstadt, Germany), equipped with a high-resolution CCD camera, a high-performance digitizing adapter (Data Physics Instruments GmbH, Filderstadt, Germany) and SCA20 software (Data Physics Instruments GmbH, Filderstadt, Germany).

2.2.11. Oxygen and water vapor permeation measurements

Oxygen permeability and water vapor measurements on circular coated PET films (50 cm^2) were performed by an isostatic permeabilimeter (mod. Multiperm, PERMTECH S.r.l., Pieve Fosciana, Italy) according to ASTM standard methods (D-3985 and F-1249 respectively). The water vapor transmission rate (WVTR) was evaluated at 25 °C/90% RH and oxygen permeability (PO_2, $cm^3\ m^{-2}\ d^{-1}$ bar^{-1}) measurements of NC-coated PET were monitored at 25 °C under 0%, 20%, 40%, 60%, 70% and 80% RH. The oxygen permeability coefficients of the NC coating alone (KPO_2, cm^3 μm $m^{-2}\ d^{-1}$ bar^{-1}) were assessed, assuming that there was no interaction between the PET and the coating layer with thickness L (μm), and that the interface between them minimally affected the permeation measurements, using the Eq. (5):

$$L/\left[KPO_{2(CNCsorMFCapscoating)}\right] = \left[1/PO_{2(coatedPETfilm)}\right] - \left[1/PO_{2(uncoatedPETfilm)}\right] \quad (5)$$

By using half-time method (Balik, 1996), the oxygen diffusion coefficient (D, $cm^2\ s^{-1}$) through the coating at each RH value was estimated according to Equation (6): $D = L^2/(7.2 \times t_{(1/2)})$, (6) where L is the thickness (cm) and $t_{1/2}$ (s) is the time required to reach half of the maximum permeability value. The oxygen solubility coefficients of the CNCs and MFC_{aps} coating (S, bar^{-1}) were estimated at each RH value by the permeability and diffusion coefficients (KPO_2 and D), based on Eq. (7)

$$S = KPO_2/D \quad (7)$$

3. Results and discussion

3.1. Optical microscopy

Fig. 1 highlights the images of neat cotton linters and APS-pretreated cotton linters.

The effect of APS is very evident as a partial defibrillation of the cotton linters that occurred during the pretreatment can easily be observed. Undoubtedly, the use of APS for pretreatment of raw materials can be considered eco-sustainable unlike other chemicals which are more toxic and dangerous for both handling and disposal. Moreover, the defibrillation can be economically viable because the number of passes through the homogenizer can be significantly reduced and also, after the pretreatment, APS residue can be reused for bleaching or pretreating raw materials even multiple times according to temperature and time monitored.

3.2. Yield of production

The yield was found to be 38%, 97% and 96% for CNCs, MFC and MFC_{aps} respectively. Indeed, these results are in straightforward accordance with our previous work (Fotie et al., 2017). Moreover, the fact that, the yields of the MFC and MFC_{aps} are similar, proves that APS pre-treatment was efficient since, it did not yield a significant production of nanoparticles.

3.3. TGA

Thermogravimetric analyses were performed in order to determine the thermal degradation/resistance of the samples. Curves are reported in Fig. 2.

Fig. 1. Images of Neat (left) and APS-pretreated (right) cotton linters recorded via optical microscopy.

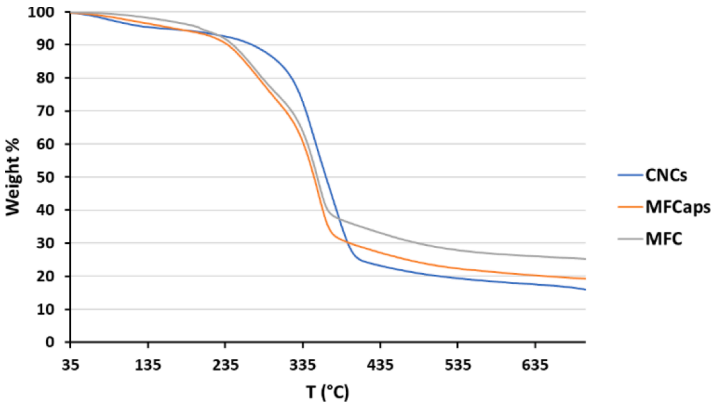

Fig. 2. Thermal degradation curves relative to CNCs, MFC_{aps} and MFC.

The three samples show different thermal degradation behaviors, according to both the different structures and surface functional groups. Table 1 reports most relevant data relative to thermal degradation by curves shown in Fig. 2, with $T_{5\%}$, $T_{50\%}$ the temperatures related to the 5 and 50% weight loss respectively.

Both MFC and MFC_{aps} show higher $T_{5\%}$ when compared to CNCs. This difference can be mainly attributed to the presence of a high number of carboxylic groups on CNC surface, deriving from the APS treatment. These acidic groups degrade at lower temperatures when compared to hydroxyl groups and also catalyze the thermally-induced water loss that contributes to the degradation mechanisms [European Polymer Journal 94 (2017) 173–184 https://doi.org/10.1016/j.eurpolymj.2017.07.014]. This same behavior was detected on MFC_{aps} in comparison to MFC. To this regard, APS pre-treated MFC show lower degradation temperatures with respect to MFC, likely due to the presence of such groups. Both MFC_{aps} and MFC are characterized by a two-step degradation profile. This behavior was attributed to the presence of both amorphous and crystalline phases that degrade at different temperatures thanks to the different packing of the chains within the nanocellulosic structure. Finally, the final residue at 700 °C was evaluated. As expected, microfibrillated cellulose derivatives showed a higher level of residue, because of the more carbon-rich structure.

3.4. WAXS crystallinity

WAXS analyses were conducted on the three samples in order to determine their crystalline structure. Fig. 3 reports the diffractograms of CNC, MFC and MFC_{aps}.

Table 1
Thermal degradation data relative to CNCs, MFC_{aps} and MFC.

Samples	$T_{5\%}$ (°C)	$T_{50\%}$ (°C)	Final residue (wt%)
CNC	143	356	15
MFC_{aps}	167	348	19
MFC	200	352	25

CNC showed a typical diffraction pattern for cellulose nanocrystals. In particular, peaks at 2θ= 14.79°, 16.58° and 22.83° were detected and associated to the Iβphase crystalline pattern of cellulose (Mascheroni et al., 2016). A similar pattern was detected for MFC samples. Both MFC_{aps} and MFC showed broader peaks in general, denouncing the higher amorphous character when compared to CNC. In particular, peaks at 2θ = 14.79°, 16.58° appeared less defined in MFC_{aps} and became a single broad peak centered at 2θ = 17.56° for MFC. Similarly, the peak at 2θ = 22.83° shifted to 22.94° and 23.52° for MFC_{aps} and MFC, respectively. These observations are in good agreement with the presence of amorphous regions in the MFC and MFC_{aps} samples with respect to CNC. On the other hand, MFC_{aps} show higher crystalline character when compared to MFC. This result suggests that the APS pre-treatment likely acts by reducing the amorphous phase of the cellulose fibers. The peak at 2θ = 29.68° in the MFC samples was assigned to the presence of spurious salts deriving from the extraction process.

3.5. Tensile strength results

Mechanical tests were performed for the determination of the tensile strength of the three cellulose-based species. Films were prepared via casting from solution and tested for their tensile strength behavior. Tensile strain at break and tensile stress at break were determined and are reported in Table 2.

CNC and MFC films showed similar behavior both considering the extensional strain and extensional stress. On the other hand, MFC_{aps} showed a higher ductility, with higher extensional strain. The lower Extensional stress expressed by MFC_{aps} in comparison to MFC, possibly denounces a lower strength of the fibers, most likely caused by the APS pre-treatment that could lead to partial degradation of the structures. The detected values are significantly lower with respect to the ones reported in literature: on one hand, when single fibers of MFC and CNC were analyzed [dx.doi.org/10.1021/bm300042t | Biomacromolecules 2012, 13, 1340−1349], the estimated Young Modulus was in the 29–36 GPa range. It should be reminded that in this paper, the Young Modulus

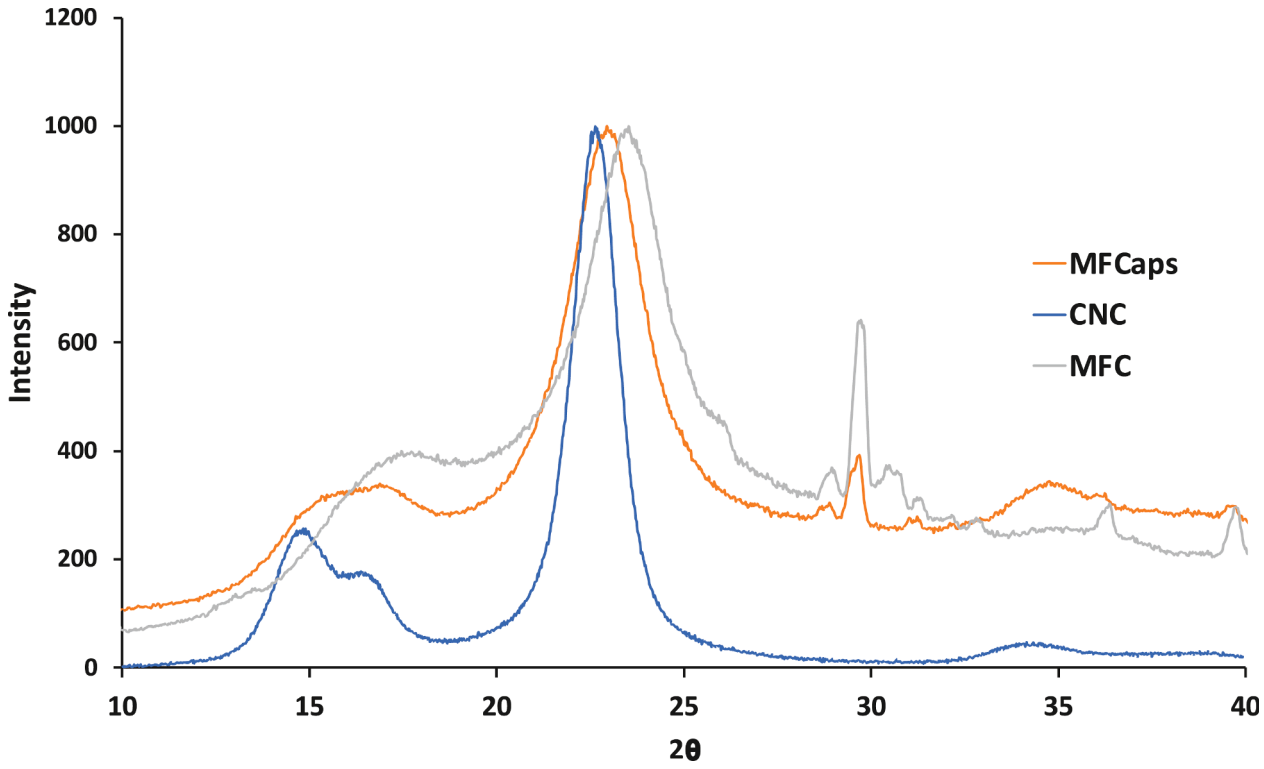

Fig. 3. Wide Angle X-ray Scattering (WAXS) diffractograms for CNCs, MFC_{aps} and MFC.

Table 2
Tensile testing data relative to CNCs, MFCaps and MFC.

Samples	Film thickness [mm]	Tensile strain at break [%]	Tensile stress at break [MPa]	Young's Moudulus (MPa)
MFC_{aps}	0.10	2.25 ± 0.10	8 ± 0.5	6 ± 0.3
CNC	0.07	1.63 ± 0.21	15 ± 0.2	14 ± 1.0
MFC	0.06	1.65 ± 0.13	15 ± 0.2	9 ± 0.7

was obtained on single fibers and was derived using different tools and analyses and it is therefore not directly comparable to the ones shown in the present paper. To this regard, values of about 0.6 Gpa were obtained in other papers on solution casted films [Composites: Part A 43 (2012) 1145–1152 doi:10.1016/j.compositesa.2012.02.006]: Moreover, in this case, the values obtained are far higher than those obtained here. A possible reason for this behavior can be found in the highly disoriented nature of the films, which probably results in a wide range of possible modulus. Solution casting doesn't allow a proper ordering of the fibers and it usually leads to the formation of random networks. In these networks, the only forces present are hydrogen bonding interactions and in some cases, only a very partial crystalline order. Young's modulus values for single fibers are significantly higher as the crystalline domains in the fibers themselves play a crucial role in determining the tensile strength of the material. In any case, in order to provide a complete explanation, we will investigate further through our future works on the same subject.

Fig. 4 reports the stress-strain curves in the elastic region.

3.6. NC properties and NC-Coated PET film

TEM images of CNCs, MFC and MFCaps can be observed in Fig. 5 and the results associated to their actual dimensions are shown in Table 3.

Results of CNCs, MFC and MFC_{aps} properties and NC-coated PET films can be observed in Table 3. As expected, values of Z potential and oxidation degree (OD) in CNCs samples were much higher, revealing the presence of the carboxylate groups reflected by the APS-oxidation, which yields a more colloidal stability. Compared to MFC, Z potential and OD values of MFCaps were slightly higher thus reflecting the presence of negative charges on the surface.

Results of NC-coated PET films assessment indicate that the MFC_{aps} layer is more than 3 times thicker than that of CNCs. In addition, haze and transparency values of the PET- MFC_{aps} were much higher and lower respectively with respect to PET- CNCs. Such diverse values are due to the larger dimensions and presence of amorphous regions within MFCaps structure, which makes PET-MFCaps much more opaque and less transparent compared to CNCs.

3.7. FTIR results

FTIR spectra of CNCs, MFC and MFC_{aps} are shown in Fig. 6. FTIR spectra are dominated by polar groups present at 3342 cm^{-1} and 1054 cm^{-1} reflecting vibrations of O—H and C—O respectively. Unlike CNCs, MFC_{aps} and MFC have intense peak at 1642 cm^{-1} that are attributable to the presence of the hemicellulose. Peak of carboxyl groups present on the CNCs and MFCaps were not revealed likely because they are less pronounced. Finally, the peak showed at around 1054–1056 cm^{-1} in all samples were related to the stretching vibrations of the cellulose.

3.8. OTR and WVTR of NC-Coated PET films

PET films coated with both CNCs and MFC_{aps} showed similar values of WVTR, 18.1 ± 1.1 and 18.3 ± 1.2 g/(m^2day) respectively, which were not different from that of uncoated PET films under the same conditions. As a result, coatings based on unmodified or hydrophilic NC cannot be used as water vapor barrier. As reported in Figs. 7, 8 and 9, oxygen permeability, Diffusion (D) and Solubility (S) coefficients were evaluated on PET film coated with cellulose nanocrystals (PET-CNCs) and microfibrillated cellulose (PET-MFC_{aps}) and are plotted with values of the relative humidity (RH). As well-known, the permeability coefficient (KP) of small molecules i.e., oxygen into coated PET films is a function of two parameters such as D and S. However, in presence of

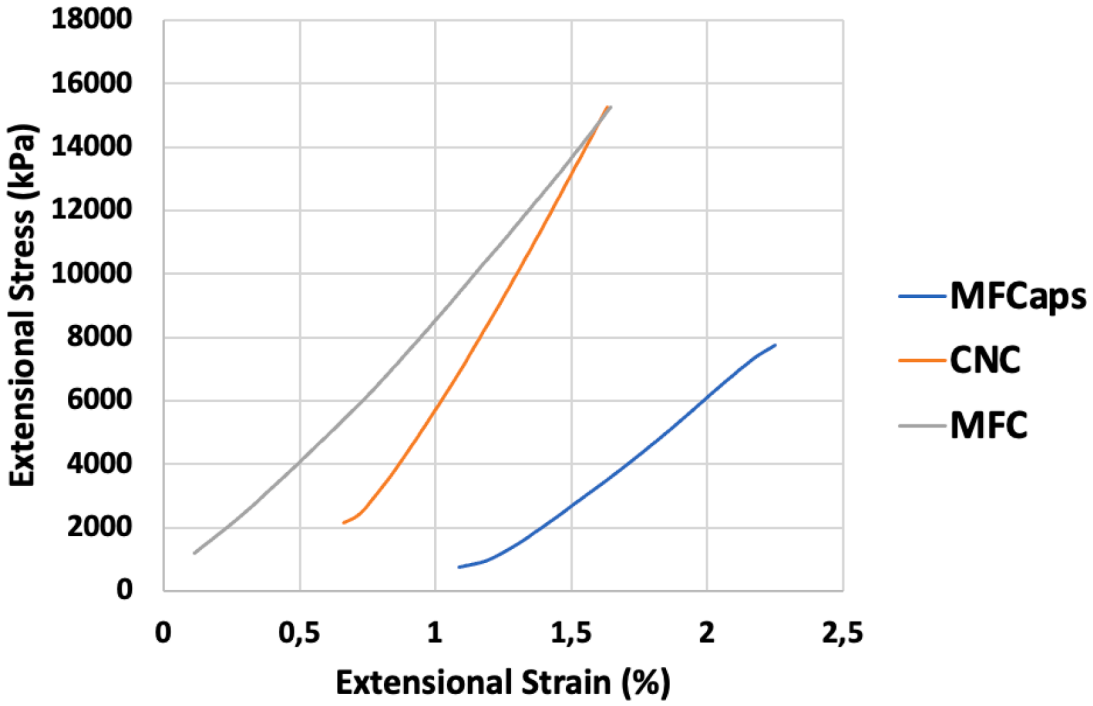

Fig. 4. Stress-strain curves of the tested samples in the elastic region.

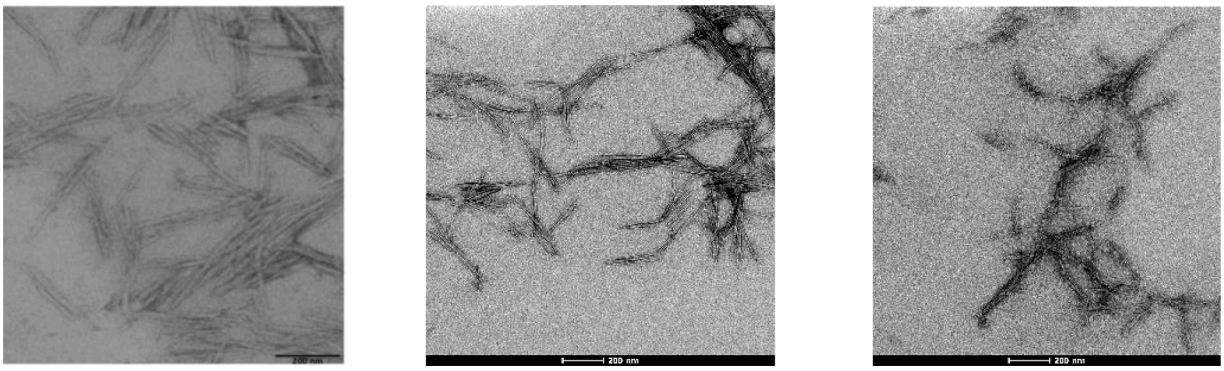

Fig. 5. TEM images of CNCs (left), MFC (middle) and MFCaps (right).

Table 3
NC Properties and NC-Coated PET films (Mean ± standard deviation).

NC properties	CNCs	MFC	MFC_{aps}
Hydrodynamic diameter (nm)	176±1.2	–	–
Average length (*L*) from TEM	139±33 nm	1–1.4 μm	1 μm
Average diameter (*D*) from TEM	16±5 nm	50±7 nm	45±5 nm
Aspect ratio (*L/D*)	9 ± 4	25±5	22±2
Zeta potential (mV)	−37.2 ± 1.1	−12±1	−17±1
Oxidation degree (OD)	0.09±0.01	0.007	0.01
Properties of NC-coated PET film		±0.001	±0.001
Thickness of uncoated PET film (μm)	12 ±0.1	–	12±0.1
Thickness of NC coating (μm)	1 ± 0.22	–	3–4
Transparency (T% at 550 nm)	88.3 ± 0.3	–	65.2 ± 0.4
Haze (%)	3.8 ± 0.1	–	54±0.2
Water contact angle (°)	26±4	–	33±4

moisture a complex mechanism reflected by three phases governs the oxygen transport through the coated PET film: dual Interaction water/oxygen (solubility) and water/CNCs, MFCaps (sorption) and transport of wet oxygen through the coated material (diffusion). It is also worth noting that the presence of a plasticizer like water plays an important role in the rate of the three above-mentioned parameters, KP increases as a result of changes in D and S. Our previous studies about the effect of humidity on the permeation of gases through nanocellulose have been reported and the results obtained are in good agreement with those ones (Fotie et al., 2017, 2018). Fig. 7 shows that PET film coated either with MFC_{aps} or CNCs exhibit much lower oxygen permeance compared to the PET alone since the crystalline network of the crystals' structure makes tortuous the passage of the oxygen molecules (Dufresne, 2013). Actually, the O_2 barrier provided by the coated film is higher 55/35 times with respect to PET alone at 0–42%RH. In addition, PET alone is almost unaffected by the moisture given its quite constant oxygen permeability values as the RH increases. By comparison with MFC_{aps}, CNCs provide a slightly better oxygen barrier at lower RH; however, its greater tendency to undergo a conformational change in presence of humidity makes them more permeable when the RH starts to increase. In fact, a higher value of water contact angle of CNCs confirms its higher hydrophilicity in comparison with MFC_{aps}. It can also be observed that, under 42% RH oxygen permeability values of PET-CNCs are slightly lower and are much greater at higher RH (> 42%). It is worth mentioning that oxygen barrier of PET-MFC_{aps} is nearly 2-fold, 2.5-fold and 1.5-fold higher than that of the PET-CNCs at 60%, 70% and 80% RH respectively. At 80% RH,

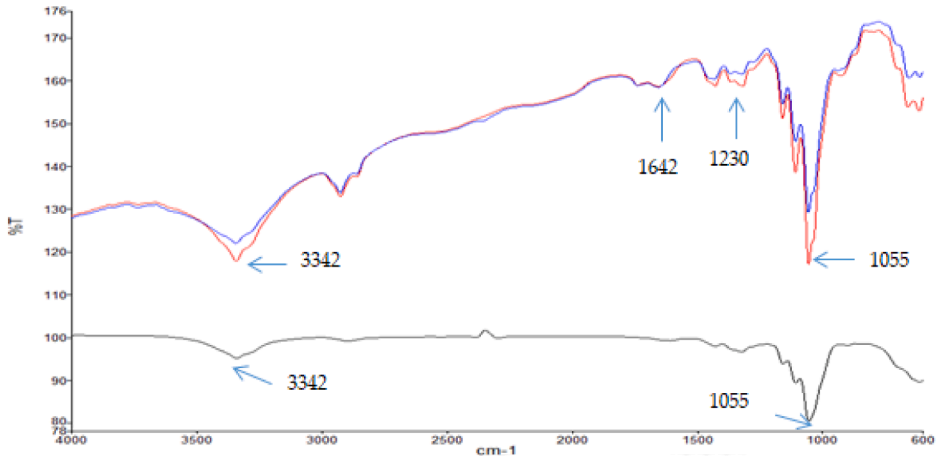

Fig. 6. FTIR spectra of MFC (blue), MFC_{aps} (red) and CNCs (gray).

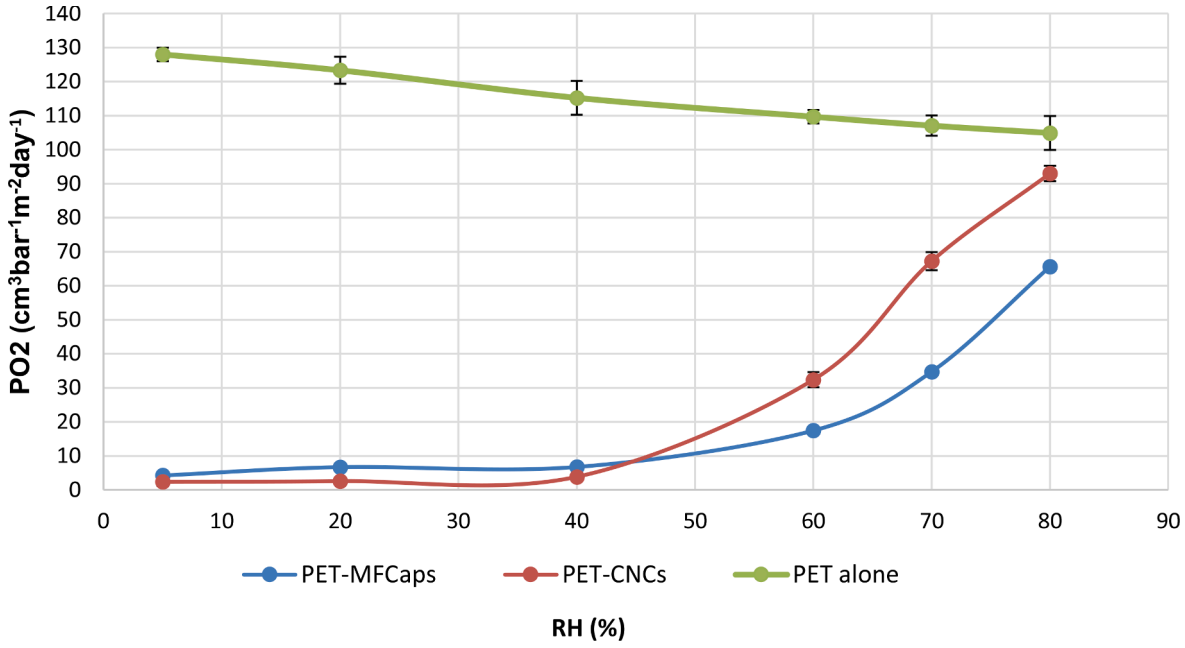

Fig. 7. Oxygen permeability as a function of RH measured on PET alone and PET coated with MFC_{aps} and CNCs.

the MFC_{aps} layer coated on the PET still provides the barrier to oxygen while that provided by CNCs layer is completely lost being almost equal to that of PET alone.

Fig. 8 shows the results of apparent diffusion coefficient (D) estimated and plotted with relative humidity values (RH). At first sight, one can observe the huge discrepancy of D values of coatings based on MFC_{aps} and CNCs. Although D values are almost constant from 0% RH to 80% RH, however, D of MFC_{aps} is approximately 15 times higher than that of CNCs. A rather elaborate explanation can be given according to Fick's law of diffusion; humidified gases diffuse faster than the dry ones do because of capillarity condensation of water molecules through the pores. In fact, the presence of moisture (RH>0) seems to have a minimal effect on the diffusion coefficient of oxygen through the materials coated with a much more cristalline structure like the CNCs (Curtis & Bird, 1999). In terms of comparison, D is far higher in MFC_{aps} because it contains amorphous regions and exhibits a lower crystallinity and density compared to CNCs.

Values of apparent solubility coefficients (S) of the samples can be observed in the Fig. 9. It can be easily noticed that S values change as the relative humidity increases. Even though this behavior was predicted theoritically, the similarity with the oxygen permeability (PO_2) is quite evident because the intersection of the S curves is also found at around 40%. From this point of view, the mixture of gases with liquids always offer a complex kinetic mechanism (Mackay & Shiu, 1981). That being said, it can be hypotesized that D contributes at the same rate to the permeation of the oxygen through layers of CNCs and MFC_{aps} from 0 to 80% RH. Therefore, from 0 to 40% RH, the oxygen permeation is driven by D because the value of S is almost null when the oxygen permeability is already 4–10 $cm^3\ bar^{-1}\ m^{-2}\ day^{-1}$. However, above 40% RH, the effect of oxygen permeability is amplified by much higher RH values and as a result, there is a strong increase in S which causes an increase of PO_2 in similar proportions.

From Fig. 9, it can be noticed that the S values of MFC_{aps} layer are almost 30 and 70 times smaller at 70 and 80%RH than those of CNCs. The first explanation is that, due to the presence of more polar functional moieties such as carboxyl ones, CNCs tend to swell more in humid environment. Considering the fact that, under similar conditions of temperature and pressure, the mixture ratio(O_2:H_2O in terms of solubility) of the wet oxygen that is about to diffuse through both samples is identical, therefore, it can be assumed that the sharp increase of S

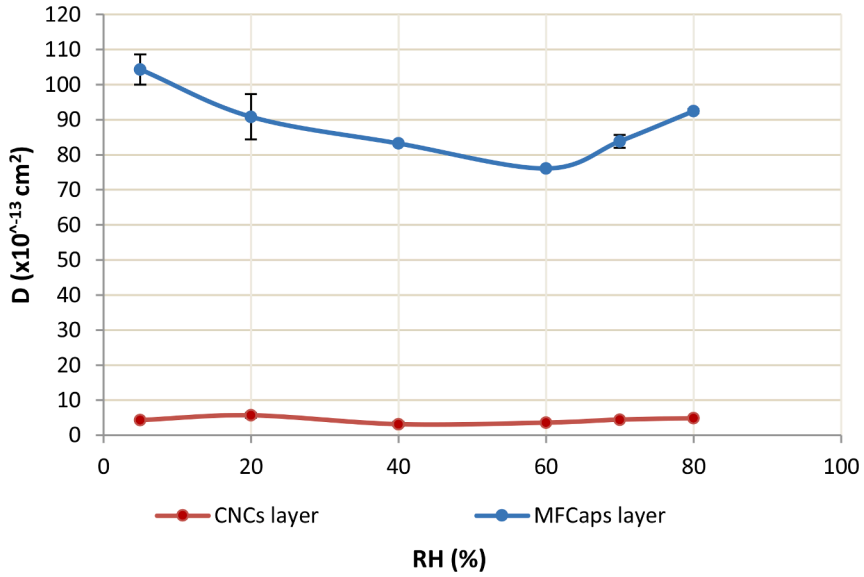

Fig. 8. Apparent diffusion coefficients of CNCs and MFC_{aps} layers versus RH.

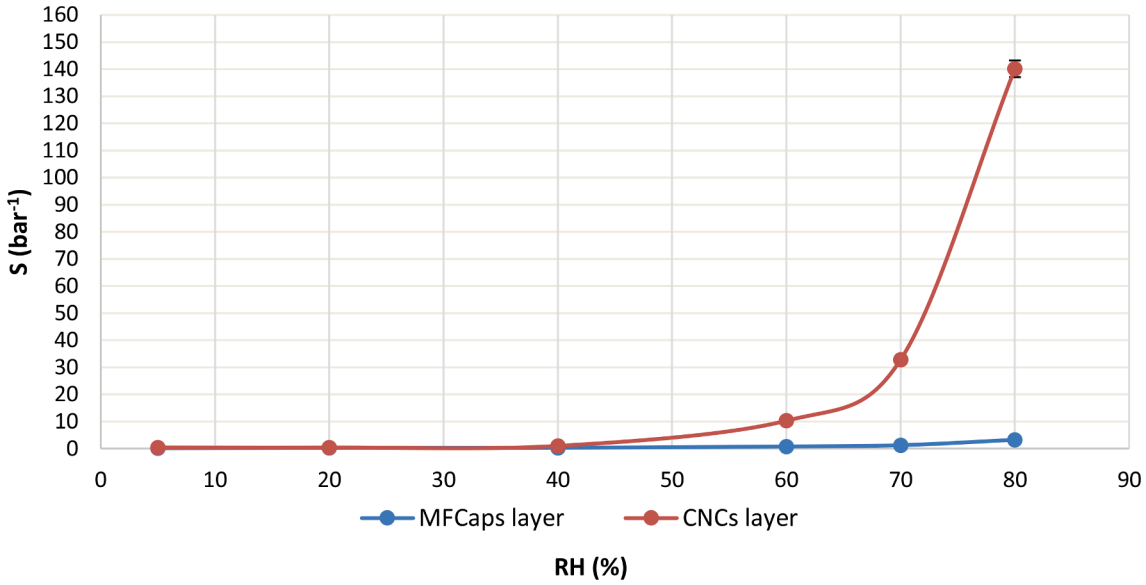

Fig. 9. Apparent solubility coefficients of CNCs and MFC_{aps} layers versus RH.

(predicted saturation) observed at 80% RH is given by additional water vapor adsorbed by CNCs layer while crossing the coated materials. To this regard, below 40% RH, oxygen permeability values (PO_2) on both CNCs and MFC_{aps} layers are very low and staying in the same order of magnitude, because their PO_2 is mainly governed by the diffusion coefficient while above 40% RH a significant increase of PO_2 values in CNCs layer is reflected by the abrupt increase in solubility coefficients. Moreover, it can be assumed that in both coating layers D values, which remain almost stable as the RH increases, slightly affect the oxygen permeation in dry and humid environment. Actually, the PO_2 increases in both layers based on MFC_{aps} and CNCs, because wet oxygen (humidified) is more prone to modify coatings' conformation and diffuses with greater ease. Finally, the better oxygen barrier obtained by MFC_{aps} layer under extremely high RH (70–80%) can be given by the two-phase mixture of MFC_{aps} structure, amorphous and crystalline, which results in a better flexibility and entanglement favoring a better resistance and tortuous pathway to the oxygen diffusion (Belbekhouche et al., 2011; Wang et al., 2020).

4. Conclusion

NC's exploitation can help create biodegradable and compostable bio-based packaging materials that meet both food security environmental and requirements concomitantly. In addition to using a nontoxic material like NC, there is a huge opportunity of creating high performance functional packaging that encompasses mechanical and gas barrier properties useful for keeping quality and extending shelf-life of foods. However, properties of the two types of NC, namely MFCaps and CNCs have to be initially assessed in order to employ them under the best conditions of applicability and to tailor a packaging as efficient as possible. The results obtained from this work revealed that CNCs coatings are more effective in blocking gas molecules only when used under conditions of low humidity, between 0 and 40% RH. For a successful scale-up of NC applications in the packaging industries, manufacturers should not only consider the economic aspects of MFCaps/CNCs such as their current market price but they should also make a decision on the packaging design according to customers' demand since opaque

coatings obtained with MFCaps and transparent ones obtained with CNCs could help develop a wide spectrum of packaging of different optical properties. In terms of functionality and machinability efficiency, to obtain an effective gas barrier, bar coating of MFCaps suspensions required more layers with respect to CNCs; moreover, the MFCaps thickness should be about 3-fold that of the CNCs. Finally, it is also relevant to indicate that without any protection of NC layer, manufacturers could adopt CNCs coatings if the packaging is to be used for foods of low water activity (aw<0.4) or/and under <40% RH whereas MFC coatings can also be used for foods with aw>0.4 and under RH>40%. However, both coatings must be confined between hydrorepellent layer under very high humid conditions. From a global perspective, it can be said that the scientific research on the nanocellulose has undoubtedly reached a crucial point that could be beneficial to packaging manufacturers who have a huge opportunity to take a disruptive approach for the development of eco-friendly bio-based food packaging in replacement of petroleum-based ones.

Funding

This research did not receive any specific grant from funding agencies in the public, commercial, or not-for-profit sectors.

CRediT authorship contribution statement

Ghislain Fotie: Conceptualization, Investigation, Methodology, Data curation, Writing – original draft. **Stefano Gazzotti:** Investigation, Methodology, Data curation, Writing – original draft. **Marco Aldo Ortenzi:** Investigation, Methodology, Data curation, Writing – original draft. **Sara Limbo:** Data curation, Formal analysis, Supervision, Writing – original draft, Validation, Visualization. **Luciano Piergiovanni:** Data curation, Formal analysis, Supervision, Writing – original draft, Validation, Visualization.

Declaration of Competing Interest

The authors declare that they have no known competing financial interests or personal relationships that could have appeared to influence the work reported in this paper

Data availability

Data will be made available on request.

References

Aulin, C., Gällstedt, M., & Lindström, T. (2010). Oxygen and oil barrier properties of microfibrillated cellulose films and coatings. *Cellulose (London, England), 17*(3), 559–574.

Balik, C. M. (1996). On the extraction of diffusion coefficients from gravimetric data for sorption of small molecules by polymer thin films. *Macromolecules, 29*(8), 3025–3029.

Belbekhouche, S., Bras, J., Siqueira, G., Chappey, C., Lebrun, L., Khelifi, B., & Dufresne, A. (2011). Water sorption behavior and gas barrier properties of cellulose whiskers and microfibrils films. *Carbohydrate Polymers, 83*(4), 1740–1748.

Dufresne, A. (2013). Nanocellulose: A new ageless bionanomaterial. *Materials today, 16*(6), 220–227.

Filipova, I., Fridrihsone, V., Cabulis, U., & Berzins, A. (2018). Synthesis of nanofibrillated cellulose by combined ammonium persulphate treatment with ultrasound and mechanical processing. *Nanomaterials, 8*(9), 640.

Fotie, G., Amoroso, L., Muratore, G., & Piergiovanni, L. (2018). Carbon dioxide diffusion at different relative humidity through coating of cellulose nanocrystals for food packaging applications. *Food Packaging and Shelf Life, 18*, 62–70.

Fotie, G., Gazzotti, S., Ortenzi, M. A., & Piergiovanni, L. (2020a). Implementation of High Gas Barrier Laminated Films Based on Cellulose Nanocrystals for Food Flexible Packaging. *Applied Sciences, 10*(9), 3201.

Fotie, G., Limbo, S., & Piergiovanni, L. (2020b). Manufacturing of food packaging based on nanocellulose: current advances and challenges. *Nanomaterials, 10*(9), 1726.

Fotie, G., Rampazzo, R., Ortenzi, M. A., Checchia, S., Fessas, D., & Piergiovanni, L. (2017). The effect of moisture on cellulose nanocrystals intended as a high gas barrier coating on flexible packaging materials. *Polymers, 9*(9), 415.

Fujisawa, S., Okita, Y., Fukuzumi, H., Saito, T., & Isogai, A. (2011). Preparation and characterization of TEMPO-oxidized cellulose nanofibril films with free carboxyl groups. *Carbohydrate Polymers, 84*(1), 579–583.

Jiang, F., & Hsieh, Y. L. (2013). Chemically and mechanically isolated nanocellulose and their self-assembled structures. *Carbohydrate polymers, 95*(1), 32–40.

Johansson, K. S. (2017). Surface modification of plastics. *Applied plastics engineering handbook* (pp. 443–487). William Andrew Publishing.

Kargarzadeh, H., Mariano, M., Huang, J., Lin, N., Ahmad, I., Dufresne, A., & Thomas, S. (2017). Recent developments on nanocellulose reinforced polymer nanocomposites: A review. *Polymer, 132*, 368–393.

Lefatshe, K., Muiva, C. M., & Kebaabetswe, L. P. (2017). Extraction of nanocellulose and in-situ casting of ZnO/cellulose nanocomposite with enhanced photocatalytic and antibacterial activity. *Carbohydrate polymers, 164*, 301–308.

Leung, A. C., Hrapovic, S., Lam, E., Liu, Y., Male, K. B., Mahmoud, K. A., & Luong, J. H. (2011). Characteristics and properties of carboxylated cellulose nanocrystals prepared from a novel one-step procedure. *Small (Weinheim an der Bergstrasse, Germany), 7*(3), 302–305.

Mackay, D., & Shiu, W. Y. (1981). A critical review of Henry's law constants for chemicals of environmental interest. *Journal of physical and chemical reference data, 10*(4), 1175–1199.

Mascheroni, E., Rampazzo, R., Ortenzi, M. A., Piva, G., Bonetti, S., & Piergiovanni, L. (2016). Comparison of cellulose nanocrystals obtained by sulfuric acid hydrolysis and ammonium persulfate, to be used as coating on flexible food-packaging materials. *Cellulose (London, England), 23*, 779–793.

Montanari, S., Roumani, M., Heux, L., & Vignon, M. R. (2005). Topochemistry of carboxylated cellulose nanocrystals resulting from TEMPO-mediated oxidation. *Macromolecules,, 38*(5), 1665–1671.

Nair, S. S., Zhu, J. Y., Deng, Y., & Ragauskas, A. J. (2014). High performance green barriers based on nanocellulose. *Sustainable Chemical Processes, 2*(1), 1–7.

Nechyporchuk, O., Belgacem, M. N., & Bras, J. (2016). Production of cellulose nanofibrils: A review of recent advances. *Industrial Crops and Products, 93*, 2–25.

Oun, A. A., & Rhim, J. W. (2018). Isolation of oxidized nanocellulose from rice straw using the ammonium persulfate method. *Cellulose (London, England), 25*(4), 2143–2149.

Ribeiro, R. S., Pohlmann, B. C., Calado, V., Bojorge, N., & Pereira Jr,, N. (2019). Production of nanocellulose by enzymatic hydrolysis: Trends and challenges. *Engineering in Life Sciences, 19*(4), 279–291.

Wang, L., Chen, C., Wang, J., Gardner, D. J., & Tajvidi, M. (2020). Cellulose nanofibrils versus cellulose nanocrystals: Comparison of performance in flexible multilayer films for packaging applications. *Food Packaging and Shelf Life, 23*, Article 100464.

Xu, X., Liu, F., Jiang, L., Zhu, J. Y., Haagenson, D., & Wiesenborn, D. P. (2013). Cellulose nanocrystals vs. cellulose nanofibrils: A comparative study on their microstructures and effects as polymer reinforcing agents. *ACS applied materials & interfaces, 5*(8), 2999–3009.

Zhang, Y., Nypelö, T., Salas, C., Arboleda, J., Hoeger, I. C., & Rojas, O. J. (2013). Cellulose nanofibrils. *Journal of Renewable Materials, 1*(3), 195–211.

Zheng, T., Zhang, Z., Shukla, S., Agnihotri, S., Clemons, C. M., & Pilla, S. (2019). PHBV-graft-GMA via reactive extrusion and its use in PHBV/nanocellulose crystal composites. *Carbohydrate polymers, 205*, 27–34.